Proceedings World Geothermal Congress 2020+1
Reykjavik, Iceland, April - October 2021

Understanding Geothermal Return Well Injectivity Decline -- the Case for Spatially Correlated Poroperm Distributions Rather Than Deep-bed Filtration

Maren Brehme

Helmholtz Centre Potsdam-GFZ German Research Centre for Geosciences, Geothermal Energy Systems, Telegrafenberg, 14473 Potsdam, Germany

Peter Leary

Advanced Seismic Instrument & Research, 1311 Waterside, Dallas, TX 75218-4475, USA
pcl@asirseismic.com

Keywords: Geothermal fluid flow, wellbore injectivity, injectivity decline, filtration

ABSTRACT

An outstanding degree of wellbore-flow asymmetry was encountered at the Klaipeda geothermal field in Lithuania. Wells that sustainably produce copious aquifer fluids are observed to clog when the wells are used as injectors -- e.g., well flow asymmetric can reach factors to 10 to 40 (a well with productivity index PI can be reduced to having injectivity index II ~ PI/40 to PI/10). A degree of reversibility is observed for freely flowing producer wells in that, while declining during temporary use as injectors, the wells can then recover full productivity. At Klaipeda, however, attempts to treat long-term injector wells – including sidetracking – failed to reverse the injectivity decline.

The observed wellbore flow asymmetry is logically due to small scale particulate matter in the injected fluid: clean produced aquifer fluids sustain flow while particulate-bearing injected fluids degrade flow. The micro-scale details of particulate clogging have not, however, been established for the Klaipeda wells, thus complicating or defeating attempts at remediation. It is typically assumed that well injectivity clogging proceeds by continuous transport of particulate matter that feeds a mass deposit that grows radially outward according to some radial profile -- a process that is often called 'deep-bed filtration'. Deep-bed filtration, with origins in the use of unconsolidated sand filters, has been given a mathematical expression involving empirical parameters that codify the unconsolidated sand filter process. Using those parameters, deep-bed filtration injectivity of large scale well flow is often assessed ('predicted') by conducting well-core-scale injectivity decline experiments using core from the given or similar well.

In our experience at Klaipeda, the deep filtration expression does not reproduce the observed decline curve. To understand this impasse, we note a fundamental distinction between filtration in (i) spatially uncorrelated porous media such as unconsolidated sands and (ii) spatially-correlated porous media such as consolidated rock. We find that an alternative physical process describes Klaipeda injector wellbore decline curve when the spatial correlation properties of the flow medium are those of rock. No match is possible for our model when the flow medium spatial correlation properties are reduced to negligible values characteristic of unconsolidated sands.

In our computation, macroscopic injectivity declines are attributed to the effects of clogging of pore-throats in proportion to the pore-throat connectivity: the greater the connectivity, the greater the flow; and the greater flow, the greater the time rate of particulate transport, and hence the greater the rate of clogging the most important flow channels. When pore connectivity distributions are lognormal, the clogging mechanism has the exponential flow decline over time, $V(t) \propto \exp(-t/\tau)$, characteristic of Klaipeda well decline data. In contrast, when the connectivity distributions are normally distributed as in unconsolidated sands, the decline curve is more characteristic of deep-bed filtration, typically of order $V(t) \propto 1/(1+t/\tau)$, that does not fit Klaipeda data.

In support of our Klaipeda decline curve modelling, we note that Klaipeda well-logs show that the geological section has crustal porosity fluctuations with power-spectra that scale inversely as a power-law in k, $P_\varphi(k) \sim 1/k$, as is observed worldwide. It is highly attested that crustal permeability κ in groundwater and other crustal flow systems is closely associated with crustal porosity φ, $\kappa \sim \exp(\alpha\varphi)$, where the value of α is such that mean product quantity has value $\langle\alpha\varphi\rangle \sim 3\text{-}4$. When porosity is spatially correlated, permeability is lognormally distributed. Such connectivity distributions lead directly to our Klaipeda decline curve results. If actual crustal wellbore decline curves are due to spatially-correlated permeability, then using well-core as diagnostic of model parameters for deep-bed filtration predictions is likely to be faulty.

1. INTRODUCTION

Decline of wellbore injectivity – ability of wellbore fluid to enter the surrounding formation -- is commonly observed in oil fields where waste water is injected into wellbores to push oil toward production wells. Fig 1 illustrates the wellbore injectivity decline trajectory over 15 years at a large offshore oil field [1]. A sequence of like injectivity declines has been observed at a direct-use geothermal system over a similar period of time (Fig 2, [2]).

As wellbore injectivity decline during oil field production forces ever higher wellhead pressures to maintain suitable injection rates, a good deal of effort has been directed at understanding the cause and potential remediation measures of wellbore injectivity [3-9]. There is wide industry agreement that injectivity decline is due principally to small scale fluid-borne particulate matter lodging in constrictions in the fluid percolation pathways of reservoir rock. We note here, however, that the standard hydrocarbon industry view of how injected particulates interact with reservoir percolation pathways is discordant with a vast array of evidence for the physical nature of percolation pathways in crustal rock.

The effect of this discordance can be summarised by the two curves shown in Fig 3. In the standard industry view, wellbore injectivity declines follow the blue hyperbolic curve, $h(t) = 1/(1+t/\tau)$. Field-scale injectivity decline data as in Figs 1-2 favour an exponential decline curve, $e(t) = \exp(-t/\tau)$ as shown in red.

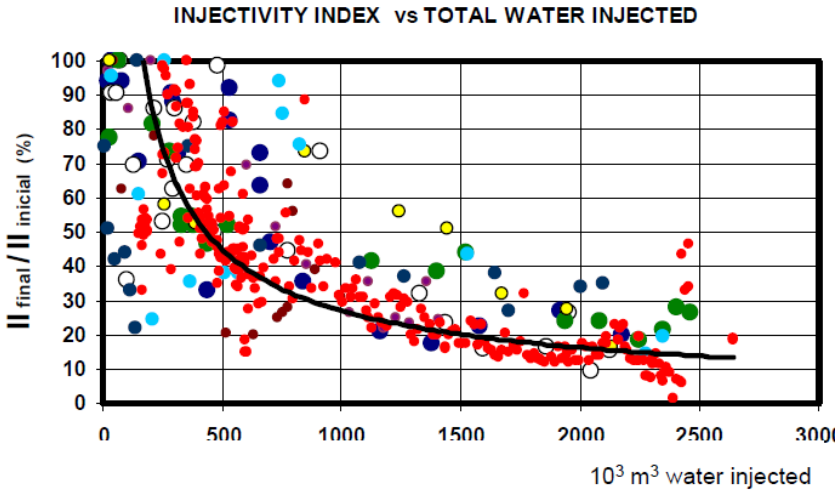

Figure 1: Black trace is mean of individual wellbore injectivity declines for 15 wells in the Campos Basin offshore hydrocarbon reservoir [1].

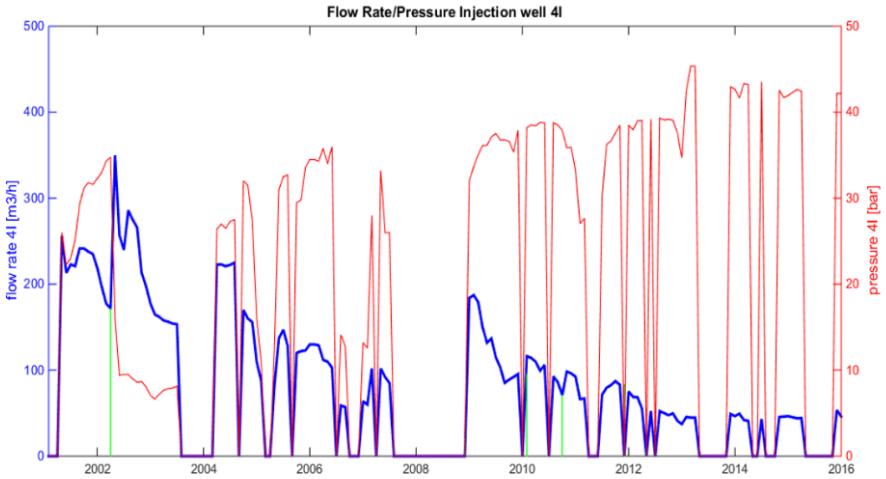

Figure 2: Blue traces record wellbore injectivity declines for injection wellbore 4I at Klaipeda geothermal field; red traces are associated wellbore injection pressures [2].

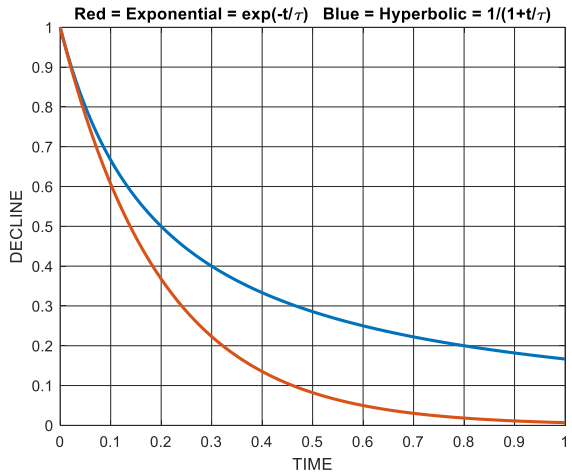

Figure 3: Type curves for wellbore injectivity decline curves as function of time. Red curve is exponential decline, $\exp(-t/\tau)$, and blue curve is hyperbolic decline, $1/(1+t/\tau)$. In each case, τ is the characteristic time span for the decline process.

Hyperbolic curves for wellbore injectivity decline arise directly from the assumption that injected particulate matter blocks crustal medium fluid flow pathways in a manner that resembles fluid filtration by unconsolidated sands. In unconsolidated sand grain assemblages, the random positions, orientations, and size of grains have no internal structure at any scale length, and as such do not provide internal structural obstacles to the passage of fluid between the grains. Particulate-bearing fluids flowing through a structureless assemblage of grains lodge particles in manner that depends only on the number of particles that have passed through any given volume element [10]. Flow-blockage scenarios based on assumed unstructured connectivity in reservoir rock yield the standard industry ''deep filtration'' approximation wellbore injectivity decline [3-9].

In contrast to the industry ''deep filtration'' process of particulate occlusion characteristic of unconsolidated material, a large array of empirical data show that consolidation processes in crustal rock induce grain-scale-connectivity structures at all scales within a crustal volume [11]. Particulate matter entering an ambient crustal rock volume with grain-scale-connectivity structures at all scales can have effects that range from the minor -- particles lodging in a small-scale flow structures that go nowhere -- to the major -- particles lodging in large-scale flow structures that are well connected to the crustal volume at large.

The Fig 3 decline curve types can be discriminated by considering the action of particulate matter in blockage of a few major flow structures versus blockage of many minor flow structures. The sharp decline of the former blockage scenario favours the exponential curve in red while a slower decline of the latter structureless scenario favours the hyperbolic curve in blue. For field-scale wellbore injectivity declines, Fig 4 shows that exponential decline curves agree with observation far better than do hyperbolic decline curves. The left-hand plot of Fig 4 compares the Fig 1 mean wellbore injectivity decline curve to a best-fit exponential curve versus a best-fit hyperbolic curve. Similarly, the right-hand plots of Fig 4 show that the three injectivity time-segments of the Klaipeda geothermal wellbore data of Fig 2 follow exponential declines, while hyperbolic declines do not reproduce the field-scale data.

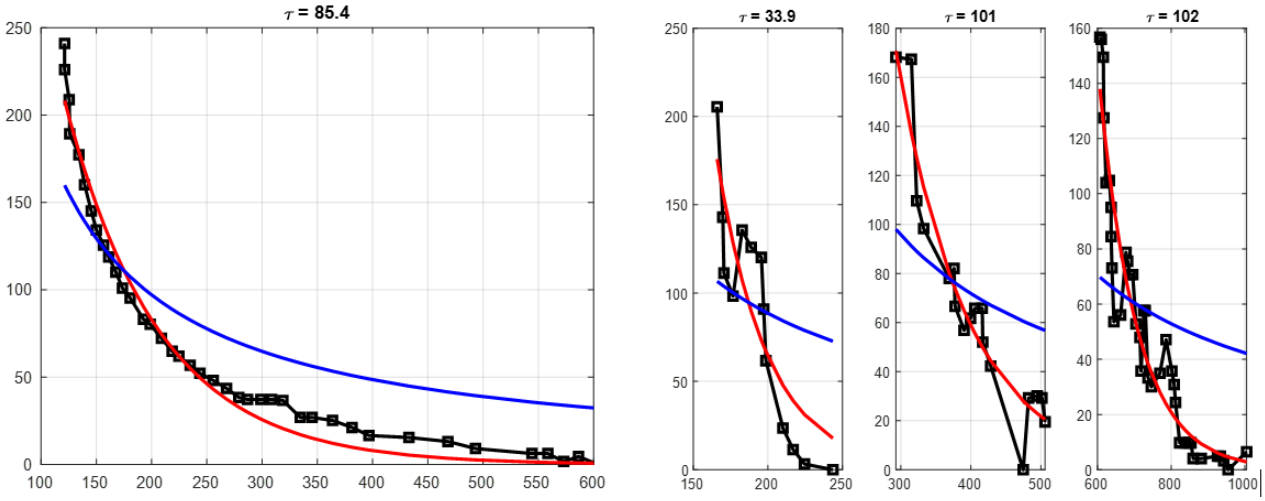

Figure 4: (Left) Digitization of Fig 1 mean Campos oil field wellbore injectivity decline curve (black) fit by exponential decline curve (red) and hyperbolic decline curve (blue). (Right) Digitization of Fig 2 Klaipeda geothermal field sequence of wellbore injectivity decline curves (black) fit by exponential decline curves (red) and hyperbolic decline curves (blue).

To examine the wellbore injectivity decline discordance illustrated in Figs 1-4, we have conducted numerical simulations of wellbore injectivity decline based on crustal rock flow empirics derived from well-logs, well-core, and well-productivity data covering length scales from cm to km. Our simulations generate exponential decline curves that agree with field-scale observation of wellbore injectivity decline. Parallel simulations based on the industry standard ''filtration model'' of particulate occlusion do not reproduce observed wellbore decline curves. We suggest that the industry standard ''deep filtration'' model is physically inaccurate and as such is potentially misleading, particularly when well-core-scale data are used to predict field-scale wellbore injection outcomes or to guide remediation of injectivity decline in producing oil fields.

The following discussion elaborates on the discrepancy between unstructured ''deep filtration'' approximation and structured empirics of fluid flow in crustal rock, then describes the computations used to simulate particulate occlusion of the systematic internal flow-structures inherent to consolidated crustal rock.

2. SPATIAL HETEROGENEITY OF CRUSTAL FLUID FLOW

In a 1956 paper celebrating the 100th anniversary of Darcy's seminal exposition of groundwater flow [12], M King Hubbert drew attention to the close parallel between Darcy's law and Ohms' and Fourier's laws of electrical thermal and conduction:

> ''…..the flow of underground fluids, is capable of being brought into the same kind of a comprehensive unification as that already achieved for the more familiar phenomena of electrical and thermal conduction.''

In drawing these parallels, Hubbert made a decisive but deeply flawed assumption that the constitutive constant in Darcy's law reflects physical processes comparable to the physical processes represented by the constitutive constant of Fourier's law. That is, Hubbert allowed himself to regard the flow of groundwater due to gravitationally-induced pressure gradients as comparable to the

flow of heat energy induced by temperature-gradients in solids. The proffered flow similarity is, however, not supported by similarities in the thermal properties of rock and the flow properties of crustal rock.

Rock thermal properties are determined by grain-grain contacts in rock's solid skeleton. As the thermal properties of silicate minerals are largely similar, and the randomness of silicate grain sizes and orientations is largely uncorrelated and additive, the bulk thermal properties of rock are normally distributed about a nominal mean with a nominal deviation from the mean of perhaps 50% [13]. Moreover, the physical grain-grain contacts in rock are easily inspected and experimented with. In contrast, the fluid flow properties of rock are decided by pore-scale connectivity effects that range from zero connectivity to high degrees of connectivity. And unlike the thermal properties of rock, it is essentially impossible to visualize or experiment with the pore-scale connectivity that permits or blocks fluid grain-scale fluid flow. Further, unlike the additive nature of thermal grain-grain contacts, connectivity processes are multiplicative in character: the absence of a single pore-pore contact can interrupt a fluid flow connectivity channel. The multiplicative nature of grain-scale fluid flow connectivity leads to lognormal distributions rather than normal distributions for bulk flow properties [11].

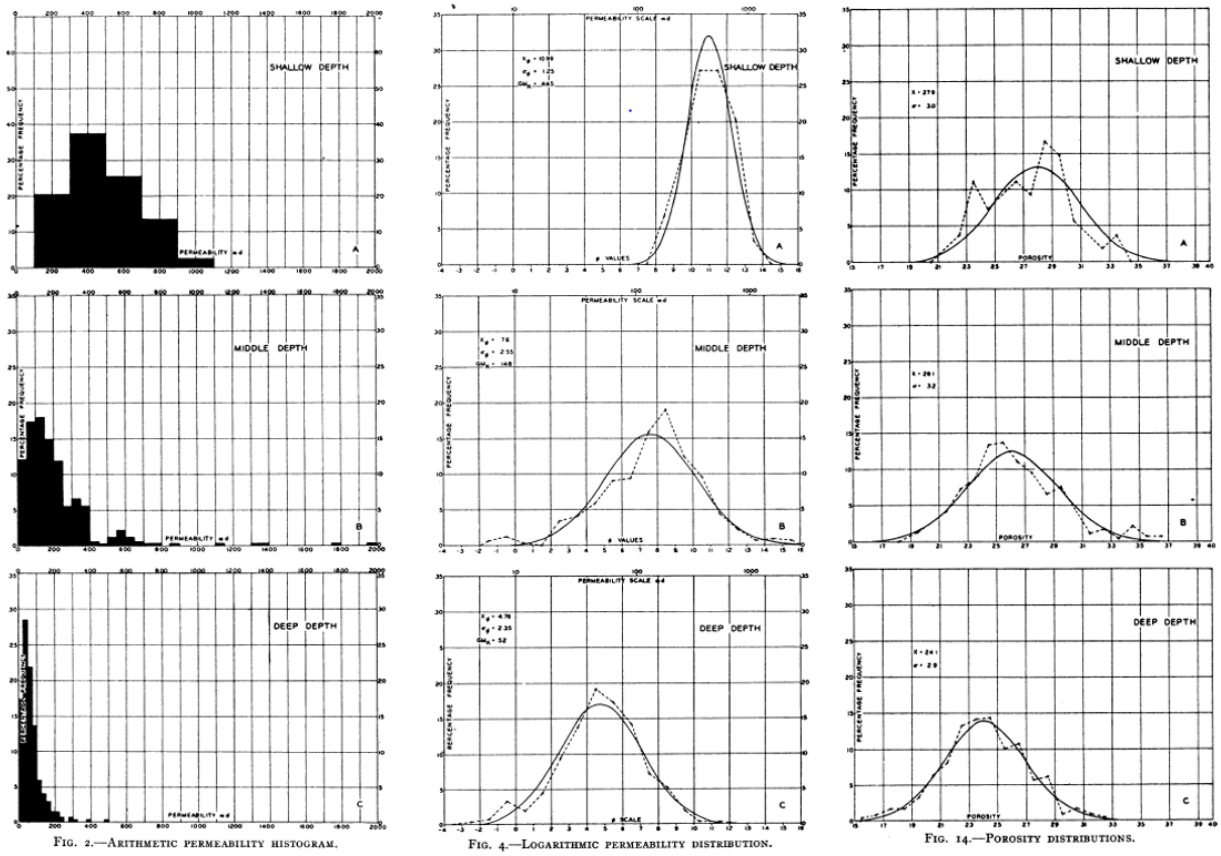

FIG. 2.—ARITHMETIC PERMEABILITY HISTOGRAM. FIG. 4.—LOGARITHMIC PERMEABILITY DISTRIBUTION. FIG. 14.—POROSITY DISTRIBUTIONS.

Figure 5: Well-core poroperm distributions for Dominguez Hills oil field in Compton, Southern California [14]. (Column left) Skew-left permeability distribution for (top to bottom) shallow, middle depth, and deep formations; (column center) normally distributed log(permeability) values; (column right) normally distributed porosity values. The center panel shows that well-core permeability conforms to the formal definition of lognormality: the distribution of log(permeability) is normal distributed.

The fundamental difference between rock's thermal properties and flow properties is exhibited in the Fig 5 set of oil field well-core data assembled by Law in 1944 [14]. Whereas the thermal properties of rock are normally distributed about a mean with a limited deviation from the mean [15], Fig 5 well-core data show that permeability in rock is lognormally distributed. Lognormal distributions of well-core permeability directly imply the existence of major connectivity pathways that dominate the flow properties of a crustal volume [11]. The characteristic large range of connectivity values documented in Fig 5 has a standard deviation of the logarithm of flow properties of 2.35 orders of magnitude. For comparison, compilations of rock thermal properties show that the standard deviation of the logarithm of thermal properties is ~ 0.1 order of magnitude [13,15].

We can immediately see how the Fig 5 difference in microscale physical processes for thermal and fluid flow manifests itself in the macroscale properties of crustal fluid flow versus heat flow. Beginning with mathematical statements of Darcy's 1856 law of fluid flow in rock, $\boldsymbol{v} = \kappa/\mu \nabla P$, and Fourier's 1822 law of heat flow for to rock, $\boldsymbol{q} = K \nabla T$, we apply the laws of conservation of fluid mass and conservation of heat energy, respectively. These conservation laws, given by $\nabla \cdot \boldsymbol{v} = 0$ and $\nabla \cdot \boldsymbol{q} = 0$, result in constraint equations $\nabla \cdot (\kappa/\mu \ \nabla P) = 0$ for fluid flow and $\nabla \cdot (K \nabla T) = 0$ for heat flow. Expanding the constraint equations with regard to Fig 5, the two physical situations are seen to be very different. Since the spatial variability of thermal properties of rock is small, the distribution of temperature is given by $\nabla^2 T = 0$, leading to spatially smooth temperature fields and corresponding heat flow fields. In contrast, fluid flow is subject to the very much more complex distributions arising from an effective ''source term'', $\nabla^2 P = -1/\kappa \ \nabla \kappa \cdot \nabla P$. While pressure seeks to be smoothly distributed, the constraint equation effective source term is subject to the strong heterogeneity evident in Fig 5.

It is thus mathematically and physically clear that, while rock temperature and heat flow are closely related in space, crustal fluid pressure and fluid flow can be quite divergent. Finite-element numerical solutions of the fluid flow constraint equation $\kappa\nabla^2 P = -\nabla\kappa\cdot\nabla P$ show that crustal fluid flow empirics create internal flow structures that can deviate strongly from the associated fluid pressure field. These heterogeneous flow structures enter decisively into the Fig 3 difference between ''deep filtration'' hyperbolic decline curves and the exponential decline curves seen in Fig 4 to agree with field-scale decline curve data.

3. DEEP FILTRATION UNCONNECTEDNESS AND THE HYPERBOLIC DECLINE CURVE 1/(1+t/τ)

In the 1930s, Muskat and co-workers examined the passage of gas through a series of artificial and natural well-core assemblages with the goal to determine if small-scale fluid flow data from reservoir rock samples could be used to reliably infer the large-scale flow properties of a reservoir system [16-18]. In their investigations, they distinguished between unconsolidated rock and consolidated rock [16]:

> *An experimental study has been made to establish quantitatively the characteristics of and laws governing the flow of gases through consolidated and unconsolidated porous materials of fine texture.*

It is straightforward logic to assume that the randomness of unconsolidated porous materials has no internal structure to complicate the extrapolation of fluid flow properties from small-scales to large-scales. If nothing else, one can shake the unconsolidated material and redo the flow measurements to check that there is no unseen structural effect. While it is far less straightforward to assume that consolidated rock has no internal structure, there is a great premium on assuming that it is possible to ignore the presence of internal structures in either or both the well-core and the field volume accessed by the wellbore:

> *.....to measure porosity, "effective" grain size, degree of cementation, etc., in an actual sand is a far greater task involving greater error than a direct measurement of the permeability factor k for a sample of the sand in question.*

In their discussion of possible structures in sandstone well-core, Muskat and coworkers focused on visible evidence of geological properties, particularly porosity, rather than considering possible grain-scale flow properties that might overprint geological properties. While in the end their laboratory results were inconclusive, a note added in proof referred to recently acquired field-scale gas flow data [16]:

> *.....[field scale] results confirm the above work.....in that.... all cases.....justify....the direct application of our analysis to field conditions.*

The assumption that reservoir rock flow properties at the well-core scale can be reliable estimators of reservoir rock flow properties at the field scale was made explicit in Muskat's 1937 treatise on fluid flow in crustal reservoirs. Writing ''I*n view....of the complete failure to attain in these investigations any result that even has a moderate range of validity and generality....*'', he goes on to write [18 §2.3]:

> *One should [take] a single constant characterizing the porous medium completely and uniquely with respect to the flow of fluids through it. This resultant constant, which completely defines dynamically the porous medium as the carrier of a homogeneous fluid in viscous motion, will be....termed the "permeability".....*

Four important and long-lasting consequences can be associated with Muskat's 1937 assertion that well-core-scale permeability measurements represent a valid estimate of an effectively homogeneous field-scale formation permeability. First, equating fluid pressure with temperature in the constraint equation $\nabla^2 P = 0$ at a stroke made fluid flow mechanics straightforward. Muskat's treatise on reservoir flow, in particular radial flow in and out of wellbores, depended on analytic expressions borrowed wholesale from the mathematics of potential theory and heat conduction in solids developed in the previous 100 years. Second, reducing fluid flow mechanics to measurement of fluid pressure gave oil and gas reservoir operators a simple physical measurement to make (fluid pressure P) as a proxy for manifestly more troublesome and costly fluid flow measurements (fluid velocity $\boldsymbol{v} = \kappa/\mu\nabla P$) required by the reservoir flow constraint equation $\nabla^2 P = -1/\kappa\ \nabla\kappa\cdot\nabla P$. Third, the expense of reservoir operations was greatly reduced if reservoir flow models required only a small number of sparsely spaced samples of reservoir permeability derived from well-core. Fluid flow $\boldsymbol{v} = \kappa/\mu\nabla P$ was then simply a multiple of the pressure gradient estimated from analytic expressions constrained by simple and tractable pressure data. Fourth, a computational-friendly approximation, pictured in Fig 6, promptly emerged in which the complexity of a crustal reservoir volume figured at the left was replaced a dual-porosity model at the right. In this substitution, relatively impermeable rock matrix cubes are assembled in an essentially uniform network of relatively permeable flow pathways [19]. The Fig 6 permeability model of crustal reservoir flow structures is populated by well-core permeability data and remains in wide use since its introduction 55 years ago [20].

Under the weight of influence of the prevailing industry view on permeability heterogeneity, treatments of wellbore injectivity decline have almost universally assumed there is little or no internal flow structure to affect permeability in either well-cores or at the field scale. In these circumstances, the 1937 mathematical formulation of ''deep filtration'' by Iwasaki for unconsolidated sand filtration of fluids has been followed. Three processes are at work in deep filtration in a core volume [10]:

i. Particulate concentration C(x) in the core falls with depth x into the core as $dC(x)/dx = -\lambda C(x)$.
ii. The accumulation V(x) of particulate matter at penetration depth x changes in time as $dC(x)/dx + dV(x)/dt = 0$.
iii. The scale constant λ changes with accumulated particular matter as $\lambda = \lambda_0 + cV(x)$.

In well-core studies of injectivity decline processes pioneered by Iwasaki, it is commonly noted that the well-core depth profile of particulate accumulations follows an exponential curve. Van Oort et al [6] summarise the deep filtration process (i)-(iii) in these terms, $dV(x)/dx = -\lambda V_0 \exp(-\lambda x)$. From this equation, they formulate an expression for the associated time-growth of filter

accumulation in terms of the volume of injected fluid required to reduce injectivity by a given fraction $f(t)$ of the initial injectivity. This expression can be in turn rewritten as a hyperbolic decline curve $f(t) = 1/(1 + t/\tau)$, where τ is the characteristic decline curve time that depends on a number of filtration process parameters [6].

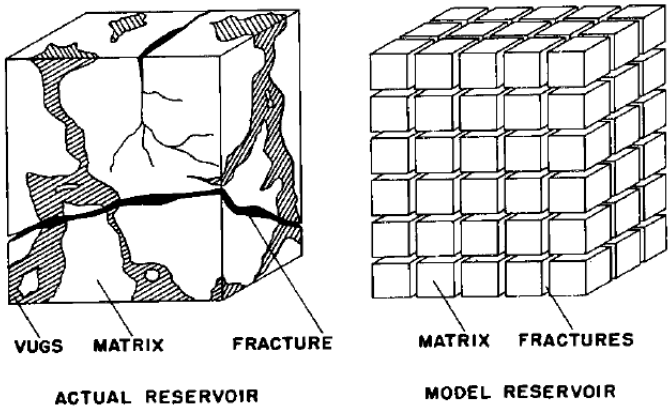

Figure 6: Despite the failure of well-core sampling to give a stable estimate of reservoir-scale permeability heterogeneity [16-18] and acknowledging the lognormal distribution of well-core permeability [14], the concept of crustal flow heterogeneity pictured at the left was reduced to a computationally tractable quasi-uniform grid approximation [19]. That reduced approximation to crustal flow heterogeneity remains standard in crustal flow simulation [20].

For the purposes of discussing wellbore injectivity decline, the key result is that the ''deep filtration process'' of Iwasaki leads to hyperbolic decline curves. The ''deep filtration model'' process, by which build-up of particulate matter occludes flow structures in rock without reference to internal flow structures, is consistent with the long-standing assumption that crustal rock flow is equivalent to flow in unconsolidated sand grain assemblages as exemplified by Hubbert [12]. In the next section, we overview the vast array of well-log, well-core, and well-production data that demonstrates that this assumed crustal permeability homogeneity has no observational basis. Incorporating well-log, well-core, and well-productivity empirics to simulate particulate occlusion processes allows for internal flow structures at all scale lengths which flow modelling shows provides exponential decline curves consistent with field scale decline data seen in Fig 4.

4. THE EMPIRICS OF CRUSTAL FLUID FLOW

If crustal permeability is not determined by the unstructured or uncorrelated randomness of unconsolidated sands, we must ask what flow structures control crustal permeability? Fortunately, abundant well-log, well-core, and well-productivity data lead us to a ''correct'' account of the spatial correlation structures arising from crustal rock-fluid interactions during consolidation.

I. From well-logs worldwide, we observe that crustal porosity fluctuation power scales inversely as a power-law in spatial frequency k, $P_\varphi(k) \sim 1/k$ [21-22];
II. From well-core worldwide, we observe that spatial variations in crustal permeability κ closely associate with crustal porosity φ as $\kappa \sim \exp(\alpha\varphi)$, with parameter α having values such that its product with mean formation porosity is of order $\alpha\underline{\varphi} \sim 3\text{-}4$ for formation porosity range $0.001 < \varphi < 0.3$ [23-24];
III. From lognormal distributions of well-productivity observed worldwide for all crustal fluids, including relic flow system mineral deposition, we observe that the well-core systematics expression $\kappa \sim \exp(\alpha\varphi)$ is effectively a lognormal distribution [25].

The overarching context for crustal consolidation that generates spatial correlation structures controlling crustal permeability is steady-state tectonic deformation acting on fluid-saturated porous rock comprised of tough mineral grains bonded by weak cements [11,24]. Residual tectonic deformation at strain rates of order 10^{-8}/yr $< \dot{e} < 10^{-7}$/yr [26] over 10^4-10^5-year intervals generate crustal strains of order $10^{-4} < e < 10^{-2}$. Tectonic strains of this order introduce irreversible finite strain damage at weak cements bonding strong mineral grains [27-29]. The essentially universal well-log spectral systematics of (I) show that on-going tectonic deformation creates in the brittle-fracture crust a wide-sense stationary random grain-scale fracture connectivity that is spatially correlated at across 6 decades of scale length, mm $< \ell <$ km. In addition to well-logs in crustal reservoir formations, neutron porosity well-logs in tight basement rock at 6km depth record spatial fluctuations with Fourier spectral power scaling inversely with spatial frequency, $S_\varphi(k) \sim 1/k$, over scale range 1/km $< k <$ 1/m. Microseismicity induced in 6km-deep basement crust and ambient microseismicity in active geothermal systems are found to be spatially correlated in precisely the manner predicted by the observed consolidation properties of crustal rock (I)-(III) [30].

The essentially universal presence of $1/k$-spectral-scaling of empiric (I) comprehensively refutes the standard assumption that crustal porosity in geological formations is effectively determined throughout the formation by a mean value and standard deviation that can be determined by a handful of small-scale samples [12], and explains why in the 1930s Muskat and coworkers could find no satisfactory understanding of gas flow through well-core [16-18]. Rather than formations having a mild quasi-uniform porosity and permeability in a formation, porosity fluctuations at all scale lengths throughout geological formations generate strongly fluctuating spatial connectivity between pores at all scales as per crustal empirics (II)-(III).

The spatial correlation properties (I)-(III) of crustal poroperm distributions generated by rock consolidation empirics are easily replicated in 2D and 3D numerical distributions. Matlab finite element solvers can generate numerical pressure field solutions to the fundamental constraint equation $\nabla^2 P = -1/\kappa\ \nabla\kappa\cdot\nabla P$ for fluid flow in an arbitrarily heterogeneous poroperm medium [11-31].

Computation of pressure and flow fields described by partial differential equation $\partial_t P = B/\mu \nabla\cdot(\kappa \nabla P) = B/\mu\ (\kappa \nabla^2 P + \nabla\kappa\cdot\nabla P)$ can be conveniently performed in 2D or 3D by the Matlab finite element PDE solver. What is required is sufficient spatial resolution to simulate the role of fractures within a *1/k*-scaling randomly fluctuating poroperm medium. This is easily achieved in 2D as illustrated by the left side of Fig 7, showing a (sparse) computational domain of an outer boundary of constant pressure/flow conditions and an inner one representing a wellbore with fixed pressure/flow initial condition. Mesh densification may produce as many as ~250000 nodes and ~500000 triangles for clear definition of fracture-connectivity in the permeability field near the wellbore. A refined version of Fig 7 (left) numerical grid creates 2D numerical distributions across 9 octaves of fluctuation magnitude spatial resolution to represent spatial variation in crustal porosity $\varphi(x,y)$. The associated permeability on the right is given by $\kappa(x,y) = \kappa_0 exp(\alpha\varphi(x,y))$ for a sufficiently large value of fracture-connectivity parameter α [24].

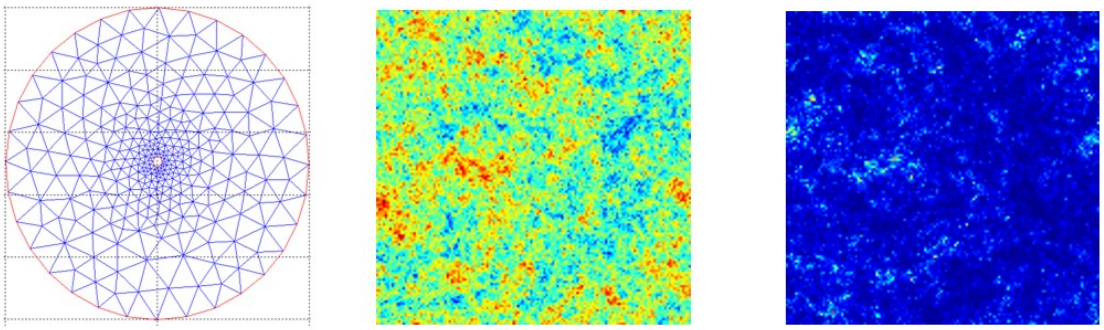

Figure 7: (Left) Representative Matlab finite element mesh used to calculating wellbore-centric pressure and velocity fields in a crustal section of poroperm media having spatial correlation distributions given by empirics (I)-(III). (Center) A 2D representation of spatially correlated porosity as given by (I). (Right) The permeability distribution as given by (II).

Figure 8 shows the steady-state pressure and flow distributions computed for a relatively large value of fracture connectivity parameter α. Fluid flow from the wellbore into the poroperm medium is dominated by a pair of fracture-connectivity pathways arising from spatially-correlated grain-scale porosity connectivity. The poroperm heterogeneity illustrated by the Fig 8 filamentary flow structure is expressed at all scales, from grain-scale to sub-well-core to reservoir scale. It is thus a clear warning that the standard viewpoint that fluid flow can be averaged over at any particular scale length is fallacious. Applying the flow characteristics illustrated in Fig 8 simulates how particulate matter operating at the grain-scale can disrupt larger scale flow in ways that are not captured by deep-bed filtration computation.

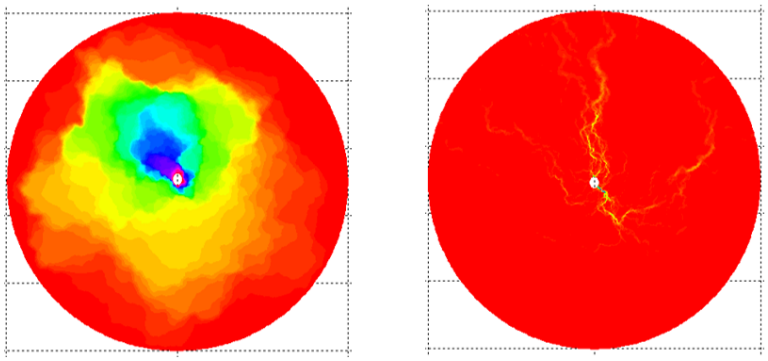

Figure 8: (Left) Pressure and (right) fluid velocity distributions resulting from a source well injecting fluid into the crustal section from a wellbore in the center of the numerical grid. Fluids bearing particulate matter can occlude a filamentary flow pattern and dramatically shut down the overall fluid flow from the wellbore into the surrounding rock, a process that has no parallel in deep-bed filtration.

5. WELLBORE INJECTIVITY DECLINE IN SPATIALLY-CORRELATED POROPERM MEDIA

The injectivity decline process due to particulate matter passing through a granular medium is treated here with specific regard to the spatially complex pore-scale connectivity structures present in crustal rock as described by rock-fluid interaction empirics (I)-(III). For a 2D crustal section centered on an injection wellbore, the initial permeability state is determined by a spatially correlated porosity field $\varphi(x,y)$ which mediates a permeability field given by $\kappa(x,y) \sim \exp(\alpha\varphi(x,y))$ in which the parameter α is taken to be constant throughout the section. As particulate-bearing fluid moves through the pore-scale connectivity structure, it is assumed that the highest velocity flow segments carry both the highest degree of fluid but also the highest degree of particular matter, and as such suffer the highest degree of particulate occlusion. It is thus assumed that for each time period of flow evolution, pore-scale connectivity structures with highest flow velocity experience a local decrement in connectivity parameter, $\alpha \rightarrow \alpha - \delta\alpha$. At each succeeding time step, a new fluid velocity field is computed to reflect fluid movement through the evolving decremented pore-scale connectivity structure.

Two variable model parameters control the computed time-evolving permeability decline: a normalised velocity threshold at which connectivity decrement occurs, and a factor by which decrement occurs. Beginning with a 100-time-step model decline curve computed for an initial model parameter setting, the velocity threshold and fractional decrement parameters are varied using the Matlab-implemented Nelder-Mead parameter search algorithm until a model decline curve is found that best fits given observed decline curve. The final model distribution of altered permeability is also obtained.

Figs 9-12 and Fig 13 illustrate the two essential results derived from models seeking to match exponential decline. First, comparing Figs 9 & 12 shows that small values of the pore-connectivity parameter α fail to simulate exponential decline, while large values of α corresponding to crustal empirics agree well with exponential decline. Second, Fig 13 shows that low values of α generate extensive deposits of particulate matter as expected from the deep-filtration model, while the permeability effects for high values of α are confined to the rim of the wellbore as occlusion of significant flow-connectivity is easily interrupted by particulate matter.

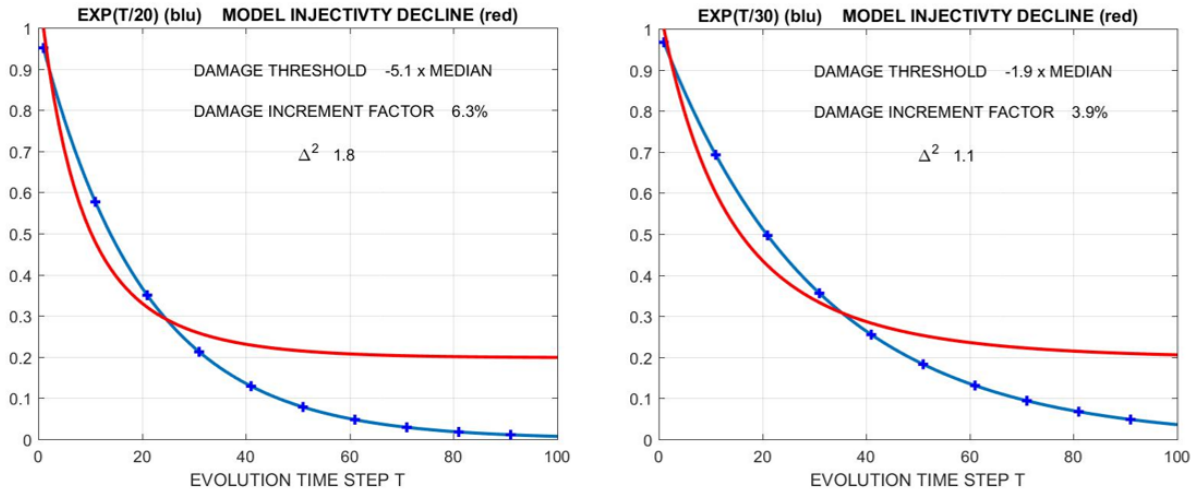

Figure 9: Modelling attempts to simulate two degrees of exponential decline (blue traces) with spatially uncorrelated poroperm property distributions governed by fracture-connectivity parameter α = 5 (red traces). Typical naturally occurring α > 20. The occlusion process for uncorrelated poroperm distributions extends deeply into the model space and ceases to increase occlusion as the model space is saturated. This result is consistent with deep filtration but is not observed in field data.

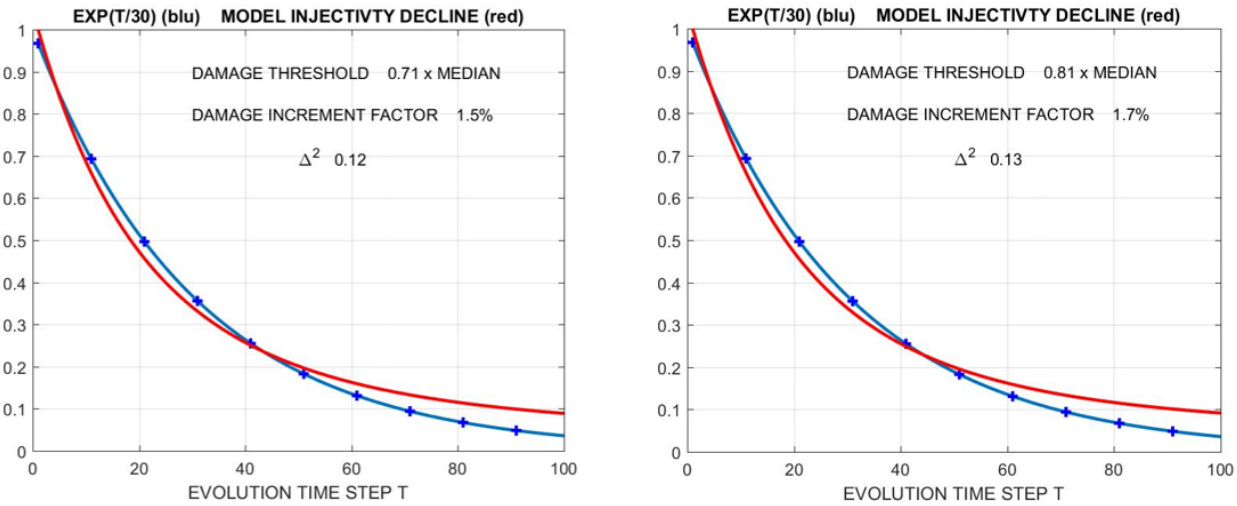

Figure 10: Modelling exponential declines (blue traces) for different realisations of moderate spatial correlation poroperm property distributions for α = 10 (red traces). Typical naturally occurring α > 20.

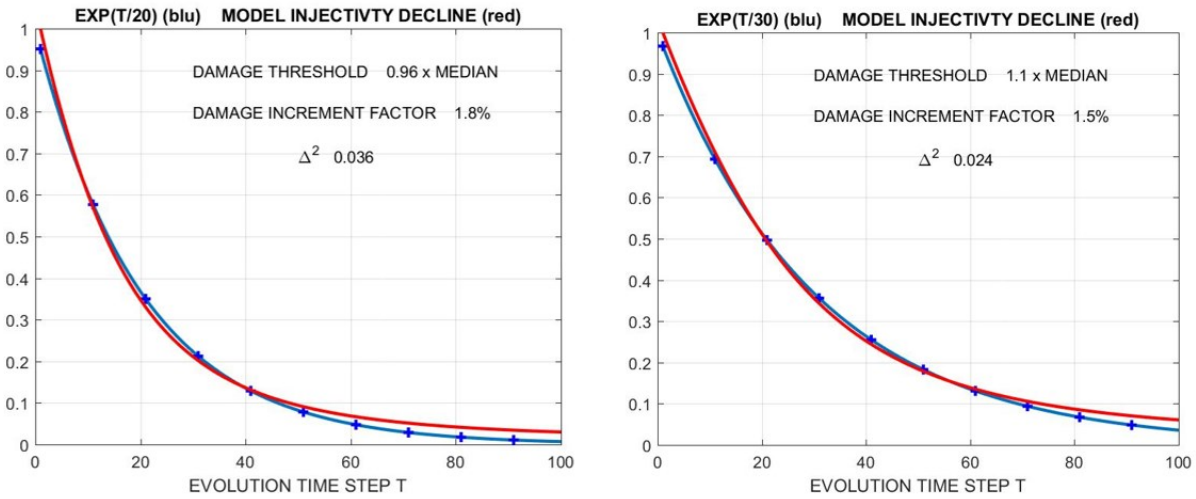

Figure 11: Modelling two degrees of exponential decline (blue traces) with moderate spatial correlation poroperm property distributions α = 15 (red traces). Typical naturally occurring α > 20.

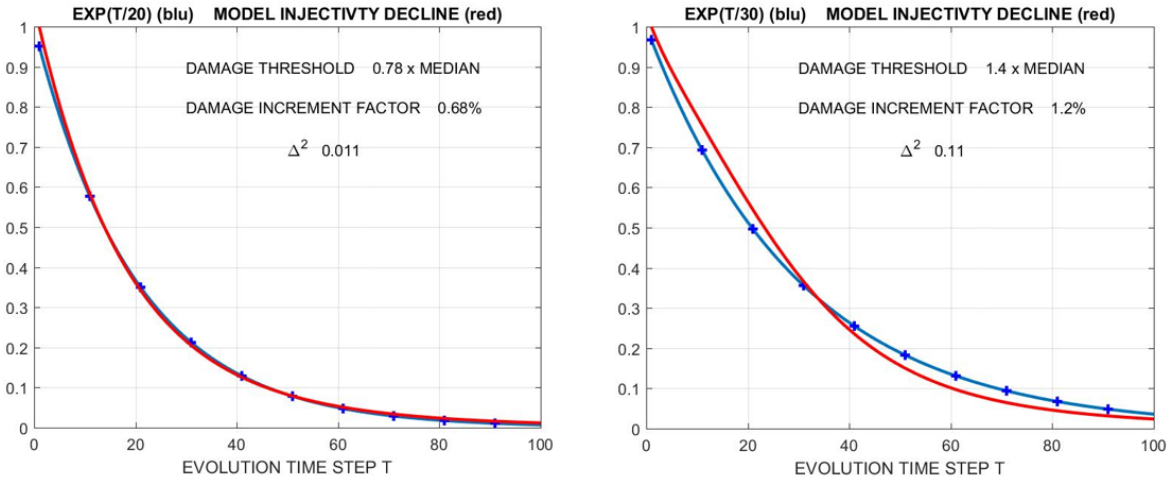

Figure 12: Modelling two degrees of exponential decline (blue traces) with strong spatial correlation poroperm property distributions α = 30 (red traces). Typical naturally occurring α > 20. Compared with the hyperbolic occlusion process of Fig 9 unconsolidated flow structures which extend injection decline indefinitely, the occlusion process of highly connected flow structures chokes off flow in the vicinity of the wellbore wall and leads to complete occlusion.

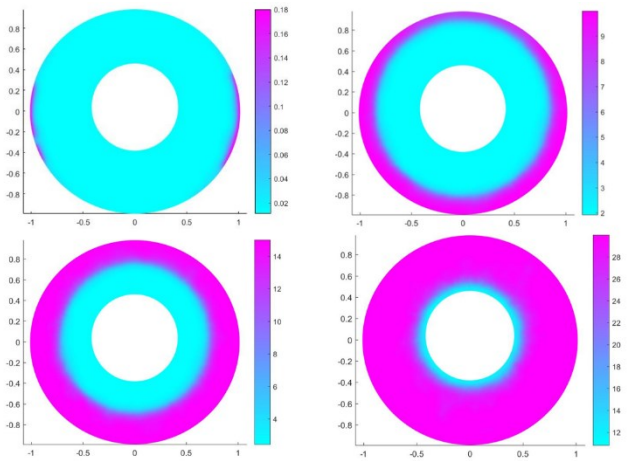

Figure 13: Radial distribution (blue tint) of occlusion-affected decline in local value of fracture-connectivity parameter α due to particulate occlusion for the four flow decline simulations of Figs 9-12. (Upper left) For α = 5 spatially uncorrelated flow structure, the ''deep filtration'' occlusion accumulation extends arbitrarily far into the surrounding formation. (Upper right, lower left) Moderate α = 10, α = 15 degrees of spatially correlated fracture-connectivity limits the radial extent of occlusion accumulation. (Lower-right). Naturally occurring α = 30 degree of spatially correlated fracture-connectivity limits the radial extent of occlusion accumulation to the immediate vicinity of the wellbore wall. The relative degree of occlusion effect is given in the color-bar to the right of each plot.

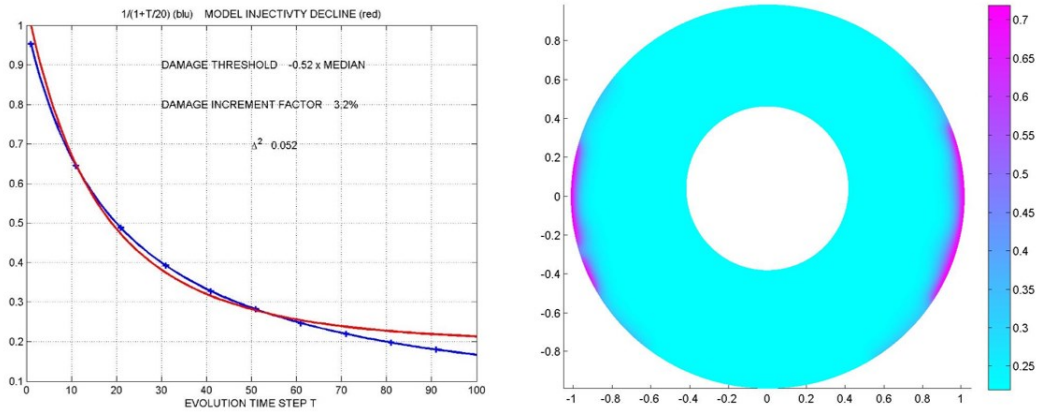

Figure 14: Modelling hyperbolic injectivity decline with α = 5 spatially uncorrelated distribution of poroperm properties confirms the present model procedure can duplicate deep-filtration occlusion for appropriate fracture-correlation parameter.

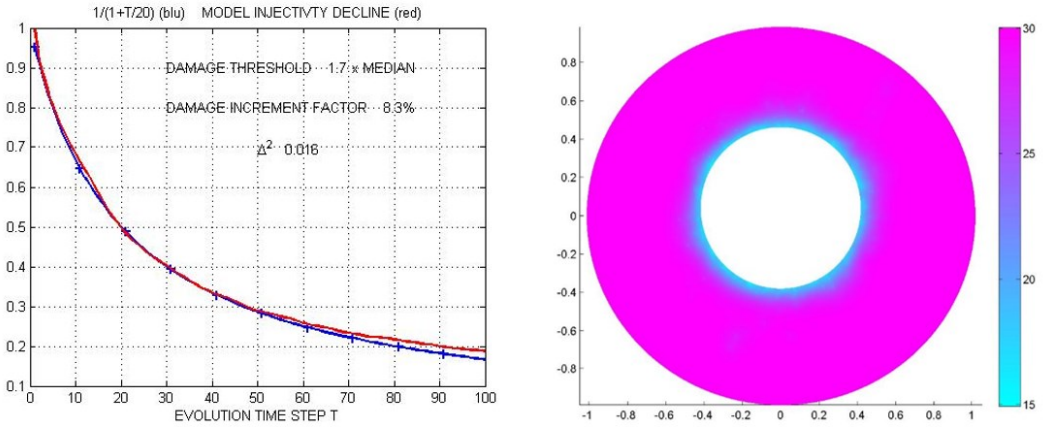

Figure 15: Modelling hyperbolic injectivity decline with α = 30 spatially correlated distribution of poroperm properties shows that compared with the Fig 12 model of exponential decline, the damage threshold and damage increment parameters must be substantially higher for hyperbolic decline than for exponential decline. That is, exponential decline indicates a greater sensitivity to the occlusion process than does a hyperbolic decline.

6. SUMMARY/CONCLUSIONS -- UNCORRELATED VERSUS CORRELATED RANDOMNESS IN CRUSTAL FLOW PROPERTIES

A decades-long effort to impose a simple engineering solution on the commercial problems arising from fluid flow complexity in crustal reservoirs has been examined and found wanting. The simple engineering solution -- that crustal flow properties vary randomly in space without involving any significant interaction at scale lengths of commercial interest -- was sketched by Hubbert [12] as reproduced in Fig 16. As the volume V of a crustal sample increases from small at the left to large at the right, spatial variations in porosity P goes through three phases: unbounded at the smallest (granular) scales, systematically drifting upwards at the largest (geological) scales, and bounded at the intermediate scales of interest to reservoir engineers. If Fig 16 is valid, then the task of running a crustal reservoir conforms to both the 1930s efforts made by Muskat and co-workers to establish that well-core samples of reservoir poroperm properties are reliably diagnostic for reservoir-scale poroperm properties [16-18], and to efforts begun in the 1970s to understand oil field waste water injectivity decline [3-9].

We have quantitatively explored the validity of efforts to explain wellbore-scale injectivity decline in terms of well-core-scale flow observations in terms of the spatially uncorrelated crustal poroperm properties sketched in Fig 16. We first noted in Figs 1-4 that field scale data exponential injectivity decline fails to conform to the hyperbolic decline curves that proceed from then Fig 16 hypothesis of spatially uncorrelated poroperm properties. We then noted that well-log, well-core, and well-productivity empirics give a strongly constrained picture of spatial correlation complexity in poroperm properties that can be readily translated into numerical flow simulation code. We find that we can numerically reproduce observed exponential injectivity decline curves, but cannot reproduce hyperbolic injectivity decline curves if we assign spatially uncorrelated poroperm properties to the computational medium. We thus conclude that, on presently available field-scale evidence, wellbore injectivity decline proceeds by a filtration process specific to poroperm spatial correlation properties consistent with the great range of well-log, well-core, and well-productivity empirics. The deep filtration hypothesis for wellbore injectivity decline is not validated by our computations.

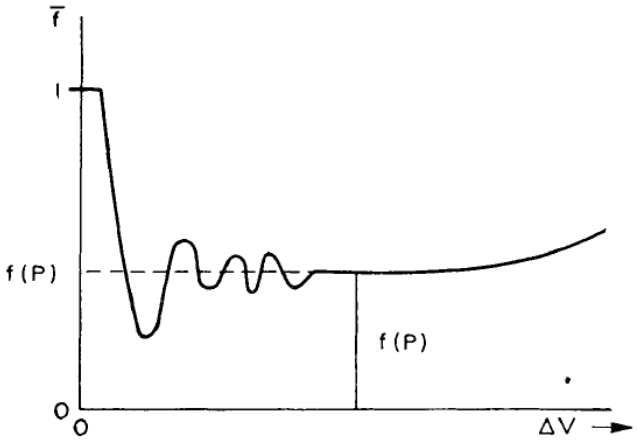

Figure 16: Scale dependence of spatial fluctuation amplitude of crustal porosity P on crustal volume scale V [12].

As a practical consequence, the different physical mechanics of particulate occlusion lead to different thicknesses of filtration matter. The spatially-uncorrelated deep filtration occlusion mechanics leads to essentially arbitrarily thick accumulations of particular matter adjacent to the wellbore. Our spatial-correction occlusion mechanics leads to thin accumulations of particular matter at the wellbore wall. Remediation of a thin accumulation of occluded matter is likely to be far more straightforward than remediating thick accumulations. While we have no specific evidence that well-core-based predictions of wellbore injectivity decline are systematically wrong, we feel justified in expressing serious doubt that these predictions are reliable. Much more relevant to wellbore injectivity decline management might be systematic field-scale evidence of the thickness of the occlusion filtrates. Our predicted thin occlusion layer should be distinguishable from deep-filtration layers, and would be potentially substantially easier to remedy.

REFERENCES

[1] Bedrikovetsky P (2009) Injectivity impairment and well & water management, Society of Petroleum Engineers Distinguished Lecturer Program, www.spe.org/dl.

[2] Brehme M, Regenspurg S, Leary P, Bulut F, Milsch H, Petrauskas S, Valickas R & Blöcher G (2018) Injection-triggered occlusion of flow pathways in geothermal operations, *Geofluids*, Vol 2018, Article ID 4694829;https://doi.org/10.1155/2018/4694829.

[3 Todd AC, Brown J, Noorkami M & Tweedie JA (1979) Review of permeability damage studies and related North Sea water injection, Society of Petroleum Engineers, SPE 7883, 211-212.

[4] Todd AC, Somerville E & Scott G (1984) The application of depth of formation damage measurements in predicting water injectivity decline, SPE 12498, 233-245.

[5] Todd AC, Kumar T & Mohammadl S (1990) The value and analysis of core-based water-quality experiments as related to water injection schemes, SPE Formation Evaluation, SPE 17148, 181-195.

[6] van Oort E, van Velzen JFO & Leerlooijer K (1993) Impairment by suspended solids invasion: Testing and prediction, SPE Production and Facilities, 8(3), 178-183; https://researchers.dellmed.utexas.edu/.../impairment-by-suspended-solids-invasion-tes...

[7] Pang S & Sharma MM (1995) Evaluating the performance of open-hole, perforated and fractured water injection wells, Society of Petroleum Engineers, SPE 30127, 489-498.

[8] Pang S & Sharma MM (1997) A model for predicting injectivity decline in water-injection wells, SPE Formation Evaluation, SPE 28489, 194-201.

[9] Sharma MM, Pang S, Wennberg KE & Morgenthaler LN (2000) Injectivity decline in water-injection wells: An offshore Gulf of Mexico case study, Society of Petroleum Engineers, SPE Prod. & Facilities, Vol. 15, No. 1, SPE 60901, 6-13.

[10] Iwasaki T (1937) Some otes onn sand filtration, *J. American Water Works Association*, Vol. 29, 1591-1602; https://www.jstor.org/stable/41231759.

[11] Leary P, Malin P & Niemi R (2017) Fluid flow and heat transport computation for power-law scaling poroperm media,

Geofluids, vol. 2017, Article ID 9687325, 12 pages.

[12] Hubbert MK (1957) Darcy's law and the field equations of the flow of underground fluids, *International Association of Scientific Hydrology, Bulletin*, *2:1*, 23-59; doi: 10.1080/02626665709493062.

[13] Clauser C & Huenges E (1995) Thermal conductivity of rocks and minerals, In: *Rock Physics & Phase Relations: A Handbook of Physical Constants*, Volume 3, Thomas J. Ahrens (Ed) https://doi.org/10.1029/RF003p0105.

[14] Law J (1944) A statistical approach to the interstitial heterogeneity of sand reservoirs, Technical Publication 1732, *Petroleum Technology* 7, May 1944.

[15] Shim BO, Park JM, Kim HC & Lee Y (2010) Statistical analysis on the thermal conductivity of rocks in the Republic of Korea, World Geothermal Congress 2010, Bali, Indonesia, 25-29 April 2010.

[16] Muskat M & Botset HG (1931) Flow of gas through porous materials, *Journal of Applied Physics* 1, 27 (1931); doi: 10.1063/1.1744983.

[17] Wyckoff RD, Botset HG, Muskat M & Reed DW (1933) The Measurement of the Permeability of Porous Media for Homogeneous Fluids, *Review of Scientific Instruments* 4, 394; doi: 10.1063/1.1749155.

[18] Muskat M (1937) *The Flow of Homogeneous Fluids through Porous Media*; McGraw-Hill: New York, NY, USA, p. 763.

[19] Warren JE & Root PJ (1963) The behavior of naturally fractured reservoirs, *Society of Petroleum Engineers Journal*, pp. 245–255.

[20] Pruess K, Oldenburg C & Moridis GJ (2012) TOUGH2 User's Guide, Version 2.1, Tech. Rep. LBNL-43134, Lawrence Berkeley National Laboratory.

[21] Leary PC (1997) Rock as a critical-point system and the inherent implausibility of reliable earthquake prediction, *Geophysical Journal International,*131, 451-466.

[22] Leary PC (2002) Fractures and physical heterogeneity in crustal rock, in *Heterogeneity of the Crust and Upper Mantle – Nature, Scaling and Seismic Properties*, JA Goff & K Holliger eds., Kluwer Academic/Plenum Publishers, New York, 155-186.

[23] Leary PC & Al-Kindy F (2002) Power-law scaling of spatially correlated porosity and log(permeability) sequences from northcentral North Sea Brae oilfield well core, *Geophysical Journal International 148*, 426-442.

[24] Leary P, Malin P, Saarno T & Kukkonen I (2018) $\alpha\varphi \sim \alpha\varphi$ crit – Basement Rock EGS as Extension of Reservoir Rock Flow Processes, *43rd Workshop on Geothermal Reservoir Engineering,* Stanford University, February 12-14, 2018 SGP-TR-213.

[25] Malin P, Leary P, Shalev E, Rugis J, Valles B, Boese C, Andrews J & Geiser P (2015) Flow Lognormality and Spatial Correlation in Crustal Reservoirs: II – Where-to-Drill Guidance via Acoustic/Seismic Imaging, WGC2015, 19-24 April, Melbourne AU.

[26] Craig TJ, Calais E, Fleitout L, Bollinger L, & Scotti O (2016) Evidence for the release of long-term tectonic strain stored in continental interiors through intraplate earthquakes, *Geophysical Research Letters 43*, doi:10.1002/2016GL069359.

[27] Trent BC & Margolin LG (1992) A numerical laboratory for granular solids, *Engineering Computations 9*, 191-197.

[28] Yin H & Dvorkin J (1994) Strength of cemented grains, *Geophysical Research Letters 21*, 903-906.

[29] Dvorkin J, Nur A & Yin H (1994) Effective properties of cemented grains, *Mechanics of Materials 18*, 351-366.

[30] Leary P, Malin P, Saarno T, Heikkinen P & Diningrat W (2019) Coupling Crustal Seismicity to Crustal Permeability – Power-Law Spatial Correlation for EGS-Induced and Hydrothermal Seismicity, *44th Workshop on Geothermal Reservoir Engineering,* Stanford University, February 11-13, 2019 SGP-TR-2141.

[31] Leary P, Malin P, Saarno T & Kukkonen I (2017) Prospects for Assessing Enhanced Geothermal System (EGS) Basement Rock Flow Stimulation by Wellbore Temperature Data, *Energies*, 10, 1979; doi:10.3390/en10121979.